Eur Biophys J (1991) 20: 87–99

European Biophysics Journal

Optical diffraction by well-ordered muscle fibres

R. A. Thornhill [1], N. Thomas [2], and N. Berovic [2]

[1] School of Biological Sciences and [2] Biophysics Group, School of Physics and Space Research, Birmingham University, Birmingham B15 2TT, United Kingdom

Received November 27, 1990/Accepted in revised form April 16, 1991

Abstract. We have studied the diffraction of a focussed laser beam by single fibres of glycerinated rabbit psoas muscle as a function of the angle of incidence. Diffraction efficiencies as high as 34% were observed at the first-order Bragg angle, indicative of well-ordered striated fibres with a strong periodic modulation of the refractive index. A theory is presented to account for our observations based upon the coupled-wave model developed by Kogelnik (1967) and Magnusson and Gaylord (1977) for the description of thick phase gratings in holography. We have solved the coupled-wave equations on a computer using a realistic index modulation taken from the measurements of Huxley and Hanson (1957). Comparison of theory with experiment shows that coupled-wave effects are indeed present in well-ordered muscle fibres, and the observed diffraction efficiency is in quite good agreement with what would be expected theoretically. Most importantly, the computer model allows us to calculate the diffraction efficiency for curved striations, which are observed for real muscle fibres under a microscope. The sensitivity of the diffraction efficiency to curvature of the striations may have implications for the interpretation of other optical experiments on muscle. We also consider the effects on our measurements of the focussing lens and refraction by the cylindrical fibre.

Key words: Muscle – Diffraction – Striations – Refractive index

Introduction

Optical diffraction by striated muscle was first reported by Ranvier (1874) over a century ago. He suggested that the regular striation pattern, which had previously been described by Bowman (1840), acted like a plane diffraction grating with a grating element equal to the sarcomere length. This simple view of diffraction by muscle endured for many years, although Sandow (1936) demonstrated that the relative intensities of the diffraction orders from whole muscle depended on the muscle thickness, and he interpreted this as evidence for multiple diffraction by successive layers of muscle fibres inside the muscle. Optical diffraction by single muscle fibres was first investigated by Buchthal and Knappeis (1940), and somewhat later the use of the diffraction pattern as a sarcomere-length gauge was developed by Blinks (1965) and by Cleworth and Edman (1969), the latter authors using a laser. However, in a length gauge it is only the *positions* of the diffraction orders which are important, and these are in fact correctly given by the simple diffraction-grating formula (Cleworth and Edman 1969) irrespective of the fibre thickness. It is when we consider the *intensities* of the diffraction orders that a more sophisticated theory is required; this, together with new experimental measurements, forms the subject of the present paper.

The effect on the diffraction pattern of the three-dimensional structure of muscle fibres themselves was neglected until relatively recently. Kawai and Kuntz (1973) investigated diffraction by single fibres but regarded them as one-dimensional gratings exhibiting negligible multiple diffraction. The three-dimensional structure of muscle fibres was considered by Fujime and Yoshino (1978) in their theoretical treatment of diffraction, but the most important breakthrough was made by Rüdel and Zite-Ferenczy (1979), who demonstrated experimentally that the intensity of a diffraction peak from a single muscle fibre is a maximum when the Bragg condition is satisfied. On the basis of this, one might regard a muscle fibre as a three-dimensional sarcomere lattice capable of producing optical Bragg diffraction analogous to the Bragg diffraction of X-rays by crystals. This analogy is, however, only partly true. In X-ray crystallography, Bragg diffraction is usually only observed at, or very near to, the Bragg angle, whilst in muscle the diffraction peaks are present at any angle of incidence (including normal incidence), just as for a diffraction grating. Therefore, although Bragg effects do indeed occur for single muscle fibres, it was recognised by Rüdel and Zite-Ferenczy (1980) and also by Baskin et al.

Offprint requests to: N. Thomas

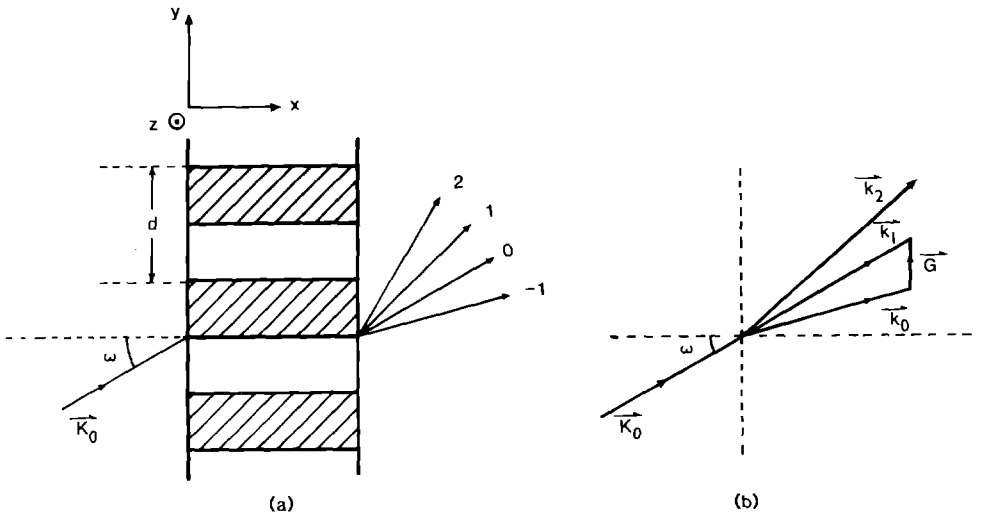

Fig. 1 a, b. A slab of cross-striated material of period d is shown in **a** together with diffraction order for $l=0, \pm 1$ and 2 arising from an incident beam of wavevector $\boldsymbol{K}_0$ at angle of incidence ω. The Cartesian co-ordinate system used in the theoretical analysis is also shown. Coupled waves with wavevectors $\boldsymbol{k}_0, \boldsymbol{k}_1, \boldsymbol{k}_2$, etc. given by (3) are produced inside the slab. These are shown in **b** together with the reciprocal lattice vector $\boldsymbol{G}$

(1981) that a quite sophisticated theory is required to account for the observed intensities of the diffraction orders. These authors realised that optical diffraction by a muscle fibre is very similar to the diffraction of light by a thick holographic phase grating, for which a theory had been developed by Kogelnik (1967) and was later extended by Magnusson and Gaylord (1977). Kogelnik's theory resolves the apparent contradiction between the Bragg and diffraction-grating viewpoints by considering in detail the propagation of light through a striated medium.

A rather different theoretical approach to this problem has recently been published by Huxley (1990). In his theory the striations are taken to act as optical waveguides. This is a perfectly correct viewpoint, but the theory has several practical disadvantages compared to the holographic approach. In the first place, the striations are taken to consist of uniform A- and I-bands, in contrast to the more complex refractive-index modulation which was determined experimentally by Huxley and Hanson (1957) for rabbit psoas muscle. Secondly, the waveguide approach becomes cumbersome away from normal incidence owing to the number of boundary conditions which have to be satisfied. Thirdly, as recognised by Huxley himself, the waveguide approach cannot readily take account of the curvature of the striation pattern, which was shown by Brenner (1985) to affect the diffracted intensity.

In this paper we show how Kogelnik's holographic theory can be applied to understand optical diffraction by well-ordered muscle fibres possessing regular cross-striations, even though these may be curved. The mathematical details are explained fully in the following section, but readers who wish to omit the mathematics may be able to understand the essential points by referring to Figs. 1–10. The remainder of the paper describes our quantitaive experimental investigation of optical diffraction by single muscle fibres. We have taken great care to eliminate optical artefacts from the experiment, and the necessary precautions are described in some detail. The results which we have obtained provide strong support for our theoretical approach. We feel that this is an important contribution not because the optical properties of muscle are themselves of direct physiological importance, but rather because optical *techniques* have been widely used for many years in phsysiological experiments without the proper physical understanding which is necessary for their correct interpretation.

Theory of diffraction by well-ordered muscle fibres

Coupled-wave theory of diffraction by a striated medium

Consider first the diffraction of light by an idealized slab of cross-striated material as shown in Fig. 1 a. Light of wave-vector $\boldsymbol{K}_0$ is incident at angle ω, and the striations of period d produce diffraction orders, some of which are shown labelled 0, ± 1, and 2. Following Kogelnik (1967), we wish to calculate the intensities of the diffraction orders by solving the wave equation for light propagation inside the striated medium. We choose a Cartesian co-ordinate system as shown, where x is normal to the slab, y is perpendicular to the striations, and z is perpendicular to the scattering plane. The light is taken to be polarized along z, parallel to the striations (so-called H-mode polarization), so that in complex notation the z-component of the electric field at time t may be written as

$$E_Z(x,y,t) = E(x,y)\exp(-j\Omega t), \tag{1}$$

where $E(x,y)$ is the complex electric-field amplitude, j is $\sqrt{-1}$, and Ω is the angular frequency of the light. The spatial part of the wave equation for E_Z is then

$$\frac{\partial^2 E}{\partial x^2} + \frac{\partial^2 E}{\partial y^2} + \frac{\Omega^2 \varepsilon(y)}{c^2} E = 0, \tag{2}$$

where c is the speed of light in vacuo, and $\varepsilon(y)$ is the optical dielectric constant of the striated medium; ε is a function of y alone because the striations are assumed to lie in the xz-plane. To gain some physical insight into this problem it is instructive to consider the wave-vector diagram shown in Fig. 1 b. In the absence of diffraction, the incident wave, whose wave-vector is $\boldsymbol{K}_0$ in the external medium, would simply be *refracted* into the zeroth-order wave of wave-vector $\boldsymbol{k}_0$ inside the slab. In the presence of

striations, however, additional *diffracted* waves are produced inside the slab with wave-vectors given by

$$\boldsymbol{k}_l = \boldsymbol{k}_0 + l\boldsymbol{G}, \tag{3}$$

where l is an integer, and $\boldsymbol{G}$ is the reciprocal-lattice vector of magnitude $2\pi/d$ directed perpendicular to the striations. As the light propagates through the medium, each diffraction order is itself diffracted by the striations, so that a set of *coupled waves* exists inside the slab. This is in essence what Sandow (1936) recognised as multiple diffraction in a whole muscle containing many muscle fibres, but, as we shall show, coupled-wave effects are in fact significant even for a *single* fibre.

The amplitude of each coupled wave changes as the light propagates through the slab. To solve the wave Eq. (2), we decompose $E(x,y)$ into coupled waves inside the slab as

$$E(x,y) = \sum_l E_l(x) \exp(j\boldsymbol{k}_l \boldsymbol{r}), \tag{4}$$

where $E_l(x)$ is the amplitude of the lth coupled wave at a distance x inside the slab, and $\boldsymbol{r}$ is the position vector of point (x,y). The dielectric constant arising from the periodic cross-striations may also be expanded in a Fourier series as

$$\varepsilon(y) = \sum_h \varepsilon_h \exp(jhGy), \tag{5}$$

where h is an integer labelling the Fourier coefficient ε_h. Substituting for $E(x,y)$ and $\varepsilon(y)$ in (2) from (4) and (5), neglecting d^2E_l/dx^2 on the assumption that $E_l(x)$ is slowly varying, we find that

$$\frac{\mathrm{d}E_l}{\mathrm{d}x} = j\frac{(k_0^2 - k_l^2)}{2k_x} E_l + \frac{j\Omega^2}{2k_x c^2} \sum_{h\neq 0} \varepsilon_h E_{l-h}, \tag{6}$$

where k_x is the x-component of the wave-vector common to all of the coupled waves inside the slab. Equation (6) is the coupled-wave equation essentially as derived by Magnusson and Gaylord (1977) following Kogelnik (1967). It is the second term on the RHS of this equation which is responsible for coupling E_l to other waves E_{l-h} whenever the Fourier component ε_h is non-zero. The first term on the RHS changes the phase of E_l, since in general $k_l \neq k_0$ inside the slab, as can be seen from Fig. 1b. Taking account of Snell's law together with (3), we find that

$$k_l^2 = k_x^2 + \frac{4\pi^2}{\lambda^2}(\sin\omega - l\lambda/d)^2, \tag{7}$$

and

$$k_x = \frac{2\pi n_0}{\lambda}(1 - \sin^2\omega/n_0^2)^{\frac{1}{2}}, \tag{8}$$

where n_0 is the average refractive index of the slab, and both the angle of incidence ω and the light wavelength λ are measured in vacuo.

The refractive-index modulation in muscle

The refractive-index modulation in single myofibrils from glycerinated rabbit psoas muscle was studied many years ago by Huxley and Hanson (1957) using interference microscopy. They found that the main contributions arise from the A- and I-filaments together with the Z-lines as shown schematically for a single sarcomere of length d in Fig. 2a. The index modulation $\Delta n(y)$ itself is drawn in Fig. 2b. It is rather more complex than the uniform A- and I-bands considered by Huxley (1990) in his waveguide approach to optical diffraction. The Fourier components of the index modulation may be determined using the equation

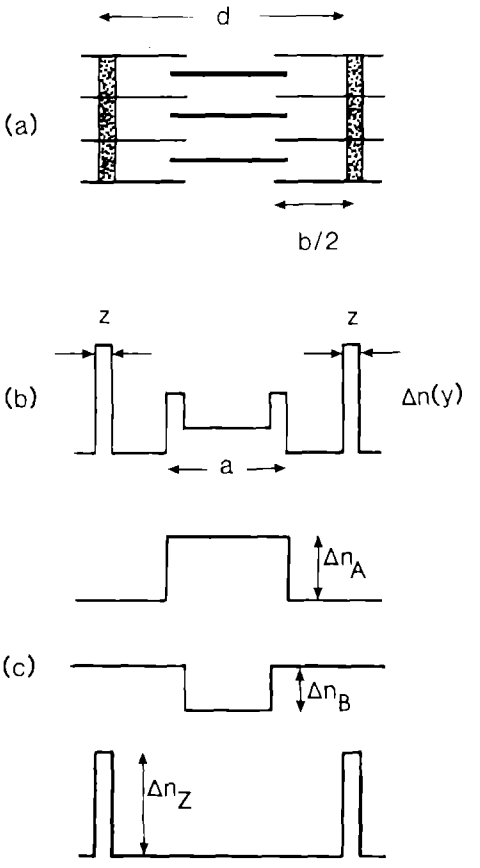

Fig. 2a–c. The structure of a single sarcomere of length d is shown schematically in **a**. The principal components are A-filaments of length a, I-filaments of length b, and Z-lines of thickness z. The overall index modulation $\Delta n(y)$ is sketched in **b**, and the individual contributions, Δn_A, Δn_B and Δn_Z, are drawn in **c** (not to scale)

$$\Delta n_h = \frac{1}{d}\int_{-d/2}^{+d/2} \Delta n(y) \exp(-jhGy)\,\mathrm{d}y. \tag{9}$$

$\Delta n(y)$ is formed from the three individual contributions as sketched in Fig. 2c: Δn_A from the A-filaments, Δn_B from the I-filaments, and Δn_Z from the Z-lines.

The dielectric constant ε is related to refractive index n by

$$\varepsilon = n^2. \tag{10}$$

Provided that the index modulation $\Delta n(y)$ is small compared to the average refractive index n_0, we can write the Fourier components of the dielectric constant (for $h \neq 0$) as

$$\varepsilon_h = 2n_0 \Delta n_h. \tag{11}$$

Analysing the three contributions to the index modulation separately leads to the following Fourier components:

$$\Delta n_{Ah} = \frac{\Delta n_A}{h\pi} \sin(h\pi a/d), \tag{12a}$$

where a is the length of the A-filaments;

$$\Delta n_{Bh} = \frac{-\Delta n_B}{h\pi} \sin[h\pi(d-b)/d], \tag{12b}$$

where b is the length of the I-filaments; and

$$\Delta n_{Zh} = \frac{z\,\Delta n_Z}{d} \cos(\pi h), \tag{12c}$$

where z, the width of the Z-line, is assumed to be much smaller than the sarcomere length d.

The absolute contribution of the muscle proteins to the refractive index was investigated by Huxley and Niedergerke (1958) for fresh single fibres of frog semitendinosus muscle. They found that the refractive index of the A-band was 0.0128 greater than that of the I-band, corresponding to a difference in protein concentration of 7.1 g/100 ml (assuming that 1 g/100 ml of protein increases the refractive index by 0.0018). This is in quite good agreement with what one would estimate for the myosin concentration based on the known structure of the thick filaments: taking the filament spacing to be 44.1 ± 0.2 nm (Brenner and Yu 1985), and assuming 6 myosins per 42.9 nm with a molecular weight of $(4.8 \pm 0.2) \times 10^5$ daltons, we estimate the myosin concentration to be 6.62 ± 0.28 g/100 ml. However, as we describe later in this paper, our actual measurements were performed on glycerinated muscle fibres mounted in a solution of 50% glycerol and 50% relaxing solution. We have determined the refractive-index increment for 1 g/100 ml of protein in this medium to be 0.00111 ± 0.00005 using an Abbé refractometer. The contribution of myosin to the refractive index is therefore estimated to be 0.0074 ± 0.0004, and this is taken to be the magnitude of the index modulation Δn_A in Fig. 2b and Eq. (12a).

To find the Fourier components of the index modulation we must include the relative weightings of the different contributions as established by Huxley and Hanson (1957). They showed that $\Delta n_A = 2\Delta n_B$, and taking $a = 1.5$ μm and $b = 2$ μm they estimated that 54.5% of the muscle protein was in the A-filaments, 36.4% in the I-filaments, and 6% in the Z-lines. Since the contribution to refractive index is proportional to the protein concentration, we estimate that $z\Delta n_Z = (6/54.5) a \Delta n_A$. Note that we have omitted any contribution from Huxley and Hanson's "S-filaments" joining the ends of the I-filaments and accounting for about 3.1% of the muscle protein. Recent work by Wang and Wright (1988) seems to show that the protein *titin* connects the Z-lines to the M-lines at the centre of the sarcomere, but if this protein is assumed to be fairly evenly distributed then it will not contribute significantly to the index modulation.

The two-beam approximation

A very useful approximate solution to the coupled-wave equation can be obtained by restricting the analysis to the interaction between the zeroth-order incident beam and the first-order diffracted beam. In this two-beam approximation the coupled-wave Eq. (6) reduces to a simple pair of differential equations:

$$\frac{dE_0}{dx} = j\varphi_1 E_1, \tag{13a}$$

and

$$\frac{dE_1}{dx} = -j\chi_1 E_1 + j\varphi_1 E_0, \tag{13b}$$

where

$$\chi_1 = \frac{k_1^2 - k_0^2}{2k_x}, \tag{14a}$$

and

$$\varphi_1 = \frac{4\pi^2 n_0 \Delta n_1}{\lambda^2 k_x}. \tag{14b}$$

The coefficients χ_1 and φ_1 therefore depend on the angle of incidence ω by virtue of equations (7) and (8) for k_1^2 and k_x.

It is straightforward to solve the coupled Eqs. (13a) and (13b) inside the striated medium subject to the boundary condition $E_1 = 0$ at $x = 0$, and thus we find that the first-order diffraction efficiency is

$$f_1(x,\omega) = \frac{|E_1(x)|^2}{|E_0(0)|^2} = \frac{4\varphi_1^2}{\chi_1^2 + 4\varphi_1^2} \sin^2[\sqrt{\chi_1^2 + 4\varphi_1^2}\, x/2]. \tag{15}$$

This equation was first derived by Kogelnik (1967) and is commonly used in the theory of volume phase holograms (see, for instance, Hariharan 1984). For given ω, (15) shows how the diffraction efficiency depends on the thickness x of the striated medium. (We assume, of course, that reflections from the boundaries of the medium may be neglected, which is a reasonable approximation in the case of a muscle fibre immersed in saline.)

It is particularly interesting to consider the diffraction efficiency at the first-order Bragg angle ω_B, which is determined by the Bragg equation

$$2d \sin\omega_B = \lambda. \tag{16}$$

In fact, when the Bragg condition is satisfied the wavevectors $\boldsymbol{k}_0$ and $\boldsymbol{k}_1$ in Fig. 1b form two sides of an isosceles triangle with the reciprocal lattice vector $\boldsymbol{G}$ along its base. In that case, $k_0 = k_1$, and the coefficient χ_1 in equation (14a) therefore vanishes. Hence, the diffraction efficiency at the Bragg angle is given by

$$f_1(x,\omega_B) = \sin^2(\varphi_1 x). \tag{17}$$

The variation of first-order Bragg intensity with thickness predicted by this equation is shown in Fig. 3, where we have taken the optical constants n_0 and Δn_1 appropriate to a muscle fibre with a sarcomere length of 3.1 μm. The

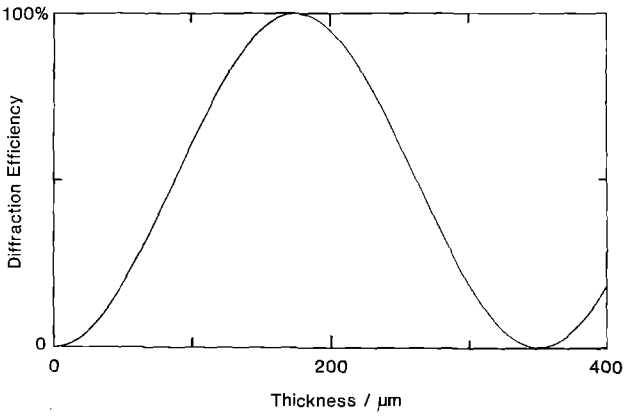

Fig. 3. Theoretical first-order diffraction efficiency f_1 at the Bragg angle as a function of thickness for a rectangular slab in the two-beam approximation according to (17). The optical parameters used were appropriate to glycerinated psoas muscle: $a=1.5$ μm, $b=2$ μm, $d=3.1$ μm, and $\Delta n_A=0.0074$. The sample is assumed to be mounted in glycerinating solution of refractive index $n_1=1.405$

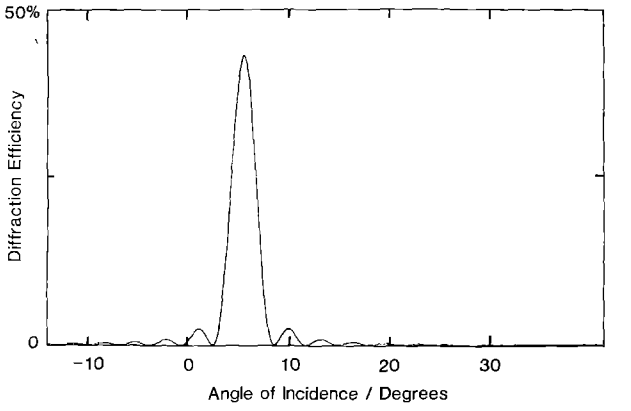

Fig. 4. Theoretical "ω-scan" showing the variation of the first-order diffraction efficiency f_1 with angle of incidence ω according to the two-beam-approximation (15). The calculation was performed for a slab of thickness 80 μm with other parameters as in Fig. 3. Note that normal incidence occurs at $\omega=0$ and the main peak occurs at the first-order Bragg angle determined by (16)

sinusoidal intensity variation is readily apparent in this figure: the diffraction efficiency reaches 100% at a thickness of about 185 μm, at which point the zeroth-order beam is completely extinguished, whilst at about 350 μm the Bragg intensity falls to zero, when all of the light has returned to the zeroth-order beam. This effect was also noted by Huxley (1990) using his waveguide theory. Similar coupled-wave behaviour is well-known in the "dynamical" theory of X-ray diffraction (see, for instance, Cowley 1975), where it is generally referred to as the *Pendellösung* effect by analogy with the behaviour of coupled pendulums. However, we prefer not to use the term "dynamical diffraction" in the case of muscle as this might cause confusion with the dynamics of muscle contraction itself.

Muscle fibres typically have thicknesses in the range of 50–100 μm. The Bragg diffraction to be expected from Fig. 3 is therefore 20–60%, so that coupled-wave effects are likely to be quite significant in optical diffraction from single muscle fibres. The high diffraction efficiency and the corresponding attenuation of the zeroth-order beam are obvious features to look for experimentally, but a more detailed test of the theory may be obtained by measuring the diffraction efficiency as a function of the angle of incidence ω to produce a so-called "ω-scan" (Baskin et al. 1981). Away from the Bragg angle, the coefficient χ_1 no longer vanishes and the theoretical diffraction efficiency in the two-beam approximation is given by (15). The predicted angular dependence of the diffraction efficiency is shown in Fig. 4 for a sample of thickness 80 μm and with other parameters as for Fig. 3. The diffraction efficiency reaches a maximum value of 43% when the angle of incidence ω is equal to the Bragg angle (in this case about 5.9°), and subsidiary peaks occur either side of this. Note that Fig. 4 does *not* imply any structure in the diffraction order itself, but rather it just shows how the intensity of the first-order diffraction peak varies with the angle of incidence. One can see from (15) that, in the case where $\varphi_1 x<\pi$, the first minima either side of the Bragg peak occur where

$$\sqrt{\chi_1^2+4\varphi_1^2}=\frac{2\pi}{x}. \tag{18}$$

In the limit of very weak modulation, φ_1 in this equation may be neglected, so that the positions of the minima are determined solely by the sample thickness x and the parameter χ_1, which is itself determined by the wave-vectors in equation (14 a). In other words, in the limit of very weak modulation the angular dependence of the diffraction efficiency is determined purely by "kinematical" conditions. One can visualize the diffraction order in this kinematical limit as arising from the interference between waves diffracted by successive thin slices within the striated medium. In this limit the minima in Fig. 4 would arise from destructive interference between the diffracted waves. (A more sophisticated view of the same process is to say that if the striated medium in Fig. 1 a has a finite thickness, then the reciprocal lattice points in Fig. 1 b should be smeared out by convolution with the Fourier transform of a top-hat function representing the slab of finite thickness x.)

In the kinematical limit, the incident wave is assumed to have a constant amplitude throughout the sample, and the diffracted wave produced by each slice of the medium is assumed not to undergo any further diffraction. Though this is the approach which is often used in elementary treatments of diffraction, it must be emphasized that the kinematical theory would not be expected to apply to well-ordered muscle fibres since the index modulation is strong enough to diffract 60% of the incident beam after a distance of about 100 μm. The angular dependence of the diffraction efficiency shown in Fig. 4 is therefore not a purely kinematical effect: the modulation parameter φ_1 not only determines the strength of the diffraction but also affects the shape of the angular dependence in Fig. 4, and in particular it determines in part the positions of the first minima through (18).

Diffraction by a medium with curved striations

In the discussion so far we have assumed that the striations are perfectly straight, but for real muscle fibres ex-

amined under a microscope some degree of curvature is generally apparent (see, for instance, Huxley and Niedergerke 1958). Brenner (1985) showed experimentally that curvature of the striations has an important effect on the diffracted intensity. The situation can be dealt with theoretically as follows. Consider a medium with a pattern of curved striations as shown in Fig. 5. Here we have introduced ripples into the striation pattern whilst maintaining the same periodicity d in the y-direction. This picture therefore represents a muscle fibre in which the sarcomere length d is well defined but where there is a regular displacement of myofibrils along the fibre axis. Mathematically the ripples in the striation pattern may be described by some curve $y=u(x)$. Hence the dielectric constant $\varepsilon(y)$ in (2) in the presence of the ripples becomes $\varepsilon(y-u(x))$. The Fourier series for this function in place of (5) is

$$\varepsilon(x,y)=\sum_h \varepsilon_h \exp[jhG(y-u(x)]\,. \tag{19}$$

So the coupled-wave equation (6) in the presence of curved striations becomes

$$\frac{dE_l}{dx}=j\frac{(k_0^2-k_l^2)}{2k_x}E_l+\frac{j\Omega^2}{2k_xc^2}\sum_{h\neq 0}\varepsilon_h E_{l-h}\exp[-jhGu(x)]\,. \tag{20}$$

We cannot in general find an analytical solution to this equation even in the two-beam approximation, so we are obliged to solve the problem by numerical methods instead. It is necessary to restrict the calculation to a finite number of beams, and for most of our numerical integrations we have worked with seven beams corresponding to $l=0$, ±1, ±2 and ±3. The main interest is still in the zeroth-order ($l=0$) and first-order ($l=\pm1$) beams, since these are readily studied experimentally, but the inclusion of coupling to the higher-order beams makes the calculation more accurate. With seven beams, the coupled-wave Eq. (20) produces seven differential equations for the complex amplitudes E_l, and for the purposes of computation these were converted to fourteen simultaneous differential equations for the real and imaginary parts of E_l. These equations were solved using a standard Runge-Kutta algorithm on an IBM PS/2 Model 70 computer fitted with an 80387 maths co-processor.

Figure 6a shows a theoretical ω-scan for the first-order diffracted beam ($l=1$) for the case of straight striations (that is, for $u=0$ in Eq. 20). We have used the same parameters as for the two-beam calculation shown in Fig. 4 to simulate a fibre of thickness 80 μm with $d=3.1$ μm, and it can be seen from comparison with

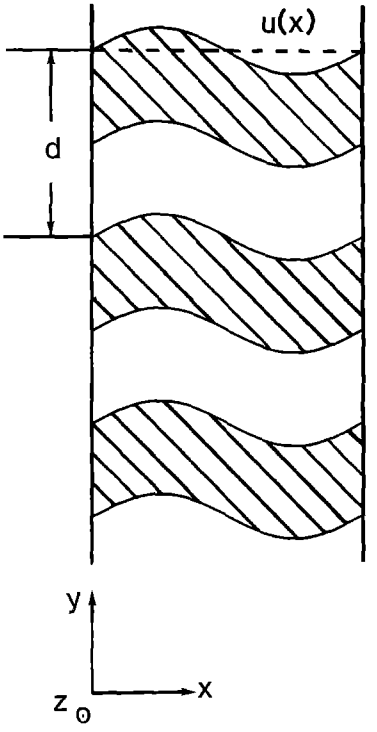

Fig. 5. A slab of cross-striated material of period d with curved striations described by $y=u(x)$. The Cartesian co-ordinate system used here is the same as in Fig. 1a

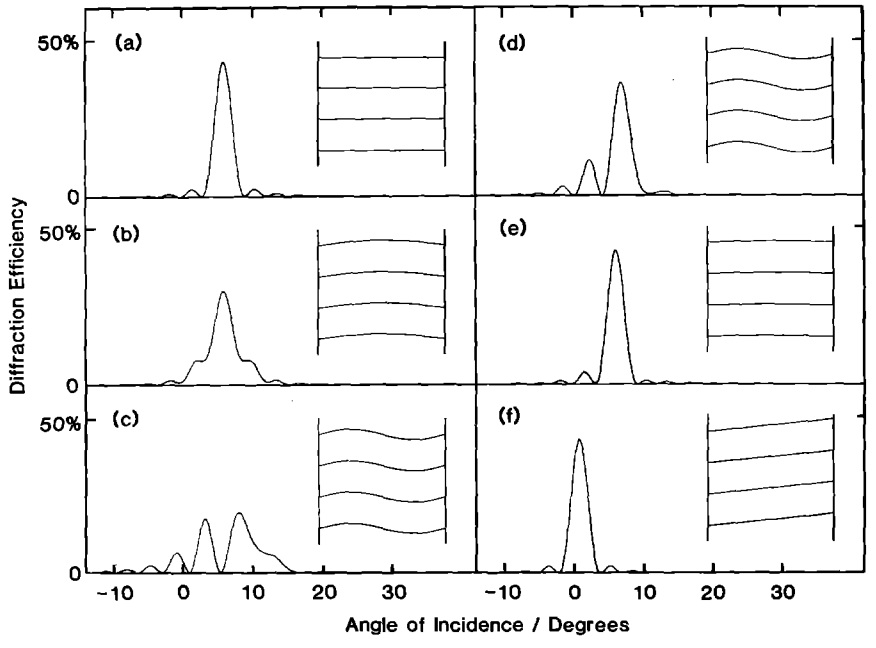

Fig. 6a–f. Theoretical ω-scans for an 80 μm slab with curved striations as sketched in each inset (not to scale). **a** shows the prediction for straight striations and is the same as Fig. 4. In **b** the striations are bowed by a sinusoidal function $u(x)$ containing a single half wavelength of amplitude 1 μm. The effect of a full-wave ripple of 1 μm amplitude is shown in **c**, whilst for **d** and **e** the amplitudes are reduced to 0.5 μm and 0.1 μm respectively. In **f**, 5 μm of skew is introduced and this shifts the Bragg peak compared to **a**

Fig. 6a that the seven-beam integration produces almost exactly the same angular dependence, especially in the important region near the Bragg angle. To examine the effect of ripples in the striations, we have used a sinusoidal displacement function of the form

$$u(x) = u_0 \sin(2\pi x/\lambda_0) . \tag{21}$$

Figure 6b shows the effect of a single half-wave ripple with amplitude $u_0 = 1$ μm and wavelength $\lambda_0 = 160$ μm; this produces the bowed striation pattern shown in the inset. The change in the angular dependence compared to Fig. 6a is immediately apparent: the subsidiary maxima either side of the Bragg angle are more intense, whilst the minima are filled in, and there is an appreciable decrease in the diffraction efficiency at the Bragg angle itself. The effect of a full-wave ripple ($\lambda_0 = 80$ μm) of the same amplitude is even more dramatic, as shown in Fig. 6c. The diffraction efficiency in this case is no longer a maximum at the Bragg angle, but instead we find that the subsidiary peaks on the left-hand side are greatly accentuated and slightly shifted to the right. The original Bragg peak has also shifted to the right, to such an extent in fact that it has merged with one of the subsidiary maxima. This trend is perhaps clearer for a full-wave ripple of 0.5 μm amplitude shown in Fig. 6d, but even with an amplitude of just 0.1 μm there is an appreciable change in the subsidiary maxima as shown in Fig. 6e.

The diffraction efficiency at any angle is clearly very sensitive to curvature of the striations. Overall we see that the effect of a full-wave ripple is to make the ω-scans in Fig. 6c–e markedly asymmetric about the Bragg angle, in contrast to the almost perfectly symmetrical angular dependence for the straight striations in Fig. 6a and the half-wave ripple in Fig. 6b. A rather different result is obtained if we introduce *skew* into the striations with a displacement function of the form $u(x) = \alpha x$. This tilts the Bragg planes, as shown in Fig. 6f for a total skew of 5 μm across the fibre; as one would expect, the Bragg peak is simply shifted relative to that in Fig. 6a since the Bragg condition in (16) is now satisfied when the incident beam makes an ange ω_B to the planes themselves rather than to the normal.

Diffraction by a cylindrical fibre

Real muscle fibres are not in fact plane slabs but are more or less cylindrical. Indeed, refraction by the cylindrical surface of a fibre was demonstrated experimentally by Marikhin and Myasnikova (1970), and its effect on the diffraction pattern needs to be considered. However, to solve the coupled-wave equation in a cylindrical geometry would be rather difficult, and we adopt instead a simpler approach based on ray optics as illustrated in Fig. 7. This figure shows a cross-section of a cylindrical fibre of radius r together with the path of a zeroth-order light ray projected onto the same plane. The wave-vector of the light ray will in general also possess a component K_y normal to this plane and parallel to the fibre axis given by

$$K_y = \frac{2\pi}{\lambda} \sin\omega , \tag{22}$$

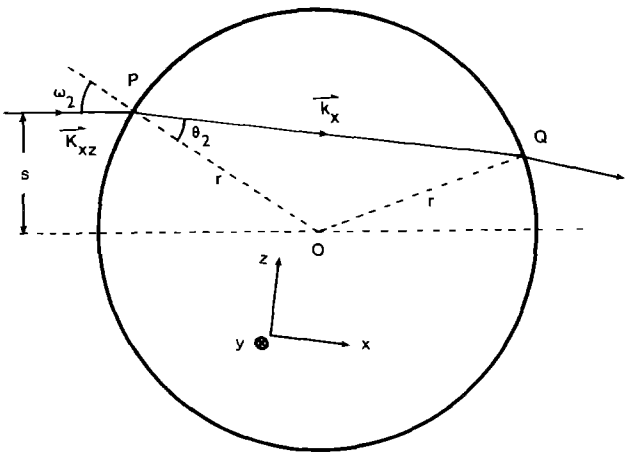

Fig. 7. Ray diagram showing refraction by a cylindrical fibre of radius r projected onto the xz diametrical plane. A ray with wave-vector component $\boldsymbol{K}_{xz}$ in this plane is incident at point P a height s above the fibre axis O and makes an angle of incidence ω_2 with the normal. The refracted ray of wavevector $\boldsymbol{k}_x$ inside the fibre makes an angle θ_2 with normal and leaves the fibre at point Q having traversed a thickness x given by (27). The Cartesian co-ordinate system used to analyse this problem is also shown

where ω is the angle of incidence projected onto the horizontal plane containing the fibre axis and the incident beam, as in the preceding theory. K_y is measured parallel to the refracting surfaces of the fibre and it is therefore *conserved* during refraction. Figure 7 shows the refraction with occurs in the xz-plane perpendicular to the fibre axis. We choose the x-axis parallel to PQ, which is the path of light beam inside the fibre projected onto the xz-plane. Snell's law for refraction in this plane at point P may be written as

$$K_{xz} \sin\omega_2 = k_x \sin\theta_2 , \tag{23}$$

where ω_2 is the angle of incidence in the xz-plane, θ_2 is the corresponding angle of refraction measured inside the fibre, and K_{xz} is the wave-vector of the incident beam in the xz-plane inside the saline of refractive index n_1 and is given by

$$K_{xz} = \frac{2\pi}{\lambda} (n_1^2 - \sin^2\omega)^{1/2} . \tag{24}$$

Note that the wave-vector component k_x inside the fibre is still given by (8).

The thickness of the fibre traversed by the ray shown in Fig. 7 is

$$x = 2r \cos\theta_2 . \tag{25}$$

It follows from the geometry that

$$\sin\omega_2 = \frac{s}{r} , \tag{26}$$

where s is the height of the incident ray above the fibre axis 0 as shown in the figure. Making use of (22)–(26) together with (8), we find that the effective thickness of the fibre for this ray is

$$x = 2r \left[1 - \frac{s^2 (n_0^2 - \sin^2\omega)}{n_0^2 r^2 (n_1^2 - \sin^2\omega)} \right]^{1/2} . \tag{27}$$

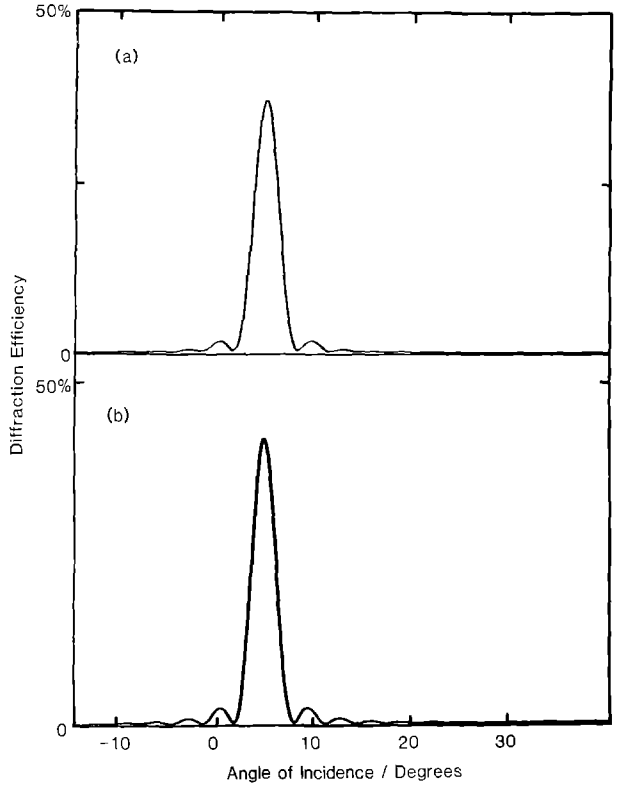

Fig. 8a, b. Theoretical ω-scans showing the first-order diffraction efficiency for a cylindrical fibre in the two-beam approximation. **a** corresponds to a broad beam described by (28b). **b** shows the behaviour for a narrow beam of 50 μm diameter, governed by (28c). The fibre was assumed to be immersed in a glycerol-saline solution of refractive index $n_1 = 1.405$, and other parameters were as for Figs. 3 and 4

The ray-optics approach is valid provided that the fibre radius r is much greater than the light wavelength λ. In that case, the incident light beam can be split into ray bundles of thickness ds, and the fibre thickness presented to each ray bundle is determined through (27) by the incident height s. The effect of striations in this model will be to set up a coupled-wave system for each ray bundle. If the whole fibre diameter is illuminated, then a fraction $ds/2r$ of the incident light lies in a ray bundle of thickness ds, and the contribution of this bundle to the first-order diffraction efficiency is

$$dF_1 = \frac{ds}{2r} f_1(x,\omega), \tag{28a}$$

which leads to the differential equation

$$\frac{dF_1}{ds} = \frac{f_1(x,\omega)}{2r}. \tag{28b}$$

Note that the right-hand side of this equation depends implicitly on the ray height s by virtue of (27).

The simplest approach to integrating (28b) is to treat the coupled waves in the two-beam approximation, in which case $f_1(x,\omega)$ is given by (15). We have performed the integration numerically using the Runge-Kutta algorithm on our PS/2 computer, and the calculated first-order diffraction efficiency F_1 for a cylindrical fibre of diameter 80 μm is shown in Fig 8a. This figure should be compared with Fig. 4, which shows the results of a two-beam calculation for a plane slab of thickness 80 μm. The effects of refraction by the cylindrical fibre are apparent in Fig. 8a: the minima in Fig. 4 are now partly filled in; the subsidiary maxima are slightly displaced; and the diffraction efficiency at the Bragg angle is somewhat reduced.

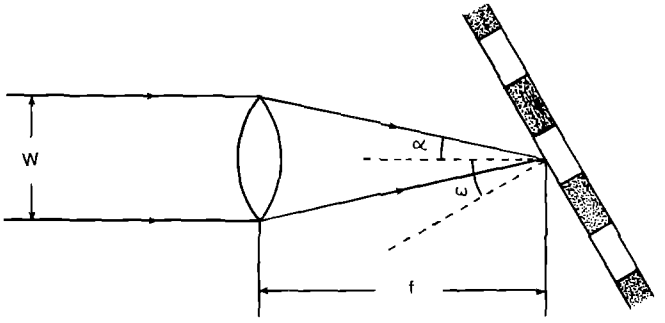

Fig. 9. Schematic diagram showing a beam of width W being focussed on to a muscle fibre by a lens of focal-length f. The nominal angle of incidence is ω as before, but rays in the focussed beam are actually incident at angles from $\omega-\alpha$ to $\omega+\alpha$. This produces some degree of angular averaging as discussed in the text

Refraction effects are reduced if we illuminate the muscle fibre with a narrow beam, so that most of the rays in the beam pass through approximately the same fibre thickness. Suppose that circular beam of width $w<2r$ is incident of the fibre. This beam should be divided into horizontal strips of width ds to define the different ray bundles, and allowing for the circular cross-section of the beam Eq. (28b) becomes

$$\frac{dF}{ds} = \frac{8}{\pi w^2}(w^2/4 - s^2)^{1/2} f_1(x,\omega). \tag{28c}$$

We have integrated this equation numerically for a beam width of 50 μm and a fibre diameter of 80 μm, and the resulting ω-scan is shown in Fig. 8b. This bears a much closer similarity to Fig. 4: the minima are no longer filled in and the diffraction efficiency at the Bragg angle is hardly reduced at all, although the subsidiary maxima are still slightly shifted. Hence by concentrating the incident beam into somewhat less than the fibre diameter we may reduce the effects of refraction.

Diffraction of a focussed laser beam

We need to use a lens to focus the incident beam down to a diffraction-limited spot on the muscle fibre. Concentrating the beam in this way reduces the effect of refraction by the cylindrical fibre, and there are also in fact some important practical advantages which are discussed in the following section. However, one important *disadvantage* of using a focussed beam must be addressed here. Figure 9 shows a ray diagram where the incident beam of width W is focussed by a lens of focal length f. The nominal angle of incidence is ω as before, but it is clear that the rays converging on the focal point are actually incident over a range of angles from $\omega-\alpha$ to $\omega+\alpha$, where α is the

half-angle subtended by the focussed beam at the fibre and is given by

$$\alpha = \tan^{-1}(W/2f) . \tag{29}$$

The lens therefore introduces some degree of angular averaging with respect to ω, and if the angular spread 2α is too large then the characteristic features of the ω-scans shown in Figs. 4, 6 and 8 will be lost.

In order to assess the effect of angular averaging on our experimental results, we have developed a somewhat simplified mathematical model. In the first place, we treat this as a two-dimensional problem and consider only the effect of focussing in the scattering plane itself. Secondly, we neglect any complications arising from diffraction by the lens and treat the focussed beam as consisting of well defined ray bundles (a valid approximation provided that $\lambda/W \ll W/f$). Thirdly, we treat diffraction by the fibre using the two-beam approximation as discussed previously. In that case, the effective first-order diffraction efficiency for the focussed beam is

$$F_1(x,\omega) = \int_{-\alpha}^{+\alpha} I(\theta) f_1(x,\omega+\theta)\, \mathrm{d}\theta , \tag{30}$$

where $f_1(x,\omega+\theta)$ defined in (15) is the first-order diffraction efficiency in the two-beam approximation for a medium of thickness x at angle of incidence $\omega+\theta$, and $I(\theta)\mathrm{d}\theta$ is the fraction of the incident intensity contained in the ray bundle focussed into the angular interval from θ to $\theta+\mathrm{d}\theta$. We make the further symplifying assumption that the laser-beam intensity before the lens is spread uniformly over the beam with W, in which case

$$I(\theta) = \frac{f}{W} \sec^2\theta . \tag{31}$$

We have evaluated the integral in (30) using (15) and (31) by means of the Runge-Kutta algorithm on our computer. A theoretical ω-scan is shown in Fig. 10 for a beam of width 1 mm focussed by a lens of focal-length 40 mm onto a plane slab of thickness 80 μm. Comparison with the corresponding ω-scan for an unfocussed beam in Fig. 4 shows that the diffraction efficiency at the Bragg angle is reduced from 43% to 40% and the subsidiary minima are partly filled in. The effects of angular averaging in this case are therefore modest because the angular spread of the incident beam (about 1.5°) is somewhat smaller than the angular width of the peak in Fig. 4. However, use of a lens with shorter focal would increase the effect of angular averaging. In practice it is therefore important to choose a lens whose focal length is only just short enough to produce a focal spot smaller than the fibre diameter.

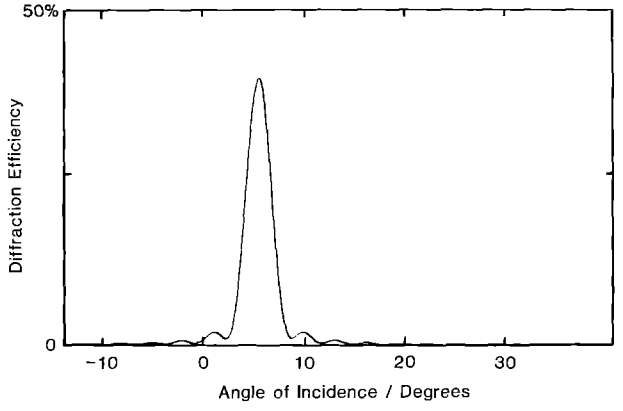

Fig. 10. Theoretical first-order ω-scan for a beam of width $W=1$ mm focussed by a lens with focal length $f=40$ mm. The other parameters are the same as for Fig. 4

Materials and methods

Fibre preparation

The muscle fibres used in this investigation were dissected from glycerinated rabbit psoas muscle, which was prepared by following the same procedure as Berovic et al. (1989). Fibres were stored at −20 °C for up to three months in a glycerinating solution consisting of 50% glycerol and 50% relaxing solution containing 3 mM ATP (Brenner 1983). We believe that the presence of ATP in the glycerinating solution helps to preserve the sarcomere order by preventing rigor. Fibres were carefully dissected in this solution without either twisting them or bending them unnecessarily. All of the fibres which we used were crystal clear when viewed under a dissecting microscope and they displayed strong irridescence in white light. Single fibres were mounted inside an optical cell (Berovic et al. 1989), which was filled with glycerinating solution. We found that fibres mounted in this solution retained their order better than those in pure relaxing solution.

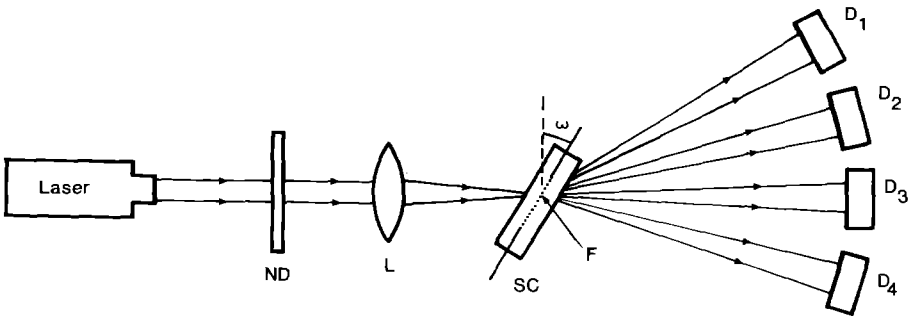

Fig. 11. Schematic diagram showing the optical apparatus used to record ω-scans from single muscle fibres. The angle of rotation ω is also shown, but note that the fibre is actually slightly offset from the centre of rotation to reduce the excursion of the laser spot. ND – neutral-density filter; L – focussing lens; SC –sample cell; F – muscle fibre; D_1–D_4 –photodiodes

Optical apparatus and procedure

The optical apparatus used for our diffraction measurements is shown in Fig. 11. The light source was a He-Ne laser (Spectra-Physics Model 120S) producing approximately 8 mW of vertically polarized light of wavelength 632.8 nm. The intensity of the light falling on the sample could be reduced with a neutral-density filter, and a lens was used for measurements with a focussed beam. Four large-area (1 cm^2) photodiodes (RS Components Ltd., Corby, Northants., UK) were used to monitor the intensities of the diffraction orders. Each photodiode signal (nominally 0.35 mA/mW) was amplified by a current-to-voltage converter to give a nominal output sensitivity of 1 V/mW. The output signals were recorded using four calibrated analogue-input channels of a BBC Model B microcomputer (Acorn Computers Ltd., Cambridge, UK) fitted with an ADC band-gap reference diode. The computer was also used to control a stepper motor, which rotated the sample cell about a vertical axis to vary the angle of incidence ω. With this equipment, "ω-scans" for up to four diffraction orders could be recorded simultaneously.

The optical quality of the muscle fibres was of prime importance, so we first examined the diffraction pattern for each fibre when it was illuminated with an unfocussed laser beam. Well-ordered fibres produced a series of sharp diffraction lines separated by a weak background of diffuse scattering, indicating that the sarcomere length d was well defined. (Occasionally what appeared to be a single fibre under the dissecting microscope turned out to be two closely associated fibres, whose diffraction lines were doublets.) The sarcomere length d was determined at this stage by measuring the separation of the first-order diffraction lines with a typical accuracy of 1%. The fibre diameter was measured using a microscope and graticule after the fibre was mounted in the sample cell.

The diffraction lines produced by muscle fibres are superficially like the "layer lines" produced by a one-dimensional periodic lattice. However, for a fibre with *three-dimensional* order these lines are in fact an artefact due to refraction by the cylindrical fibre (Marikhin and Myasnikova 1970). Close inspection shows that the intensity in the diffraction lines is concentrated along the meridian, and when a focussed laser beam is used a series of meridional diffraction spots is obtained instead of the diffraction lines. The meridional spots can also be used to test for skew in the fibre. In the absence of skew the meridian is horizontal, and at normal incidence the intensities of right-hand and left-hand diffraction order ($\pm l$ in the preceding theory) should be equal (assuming no curvature in the striations). The effect of skew may be either to tilt the meridian relative to the horizontal or to produce left-right asymmetry in the diffracted intensities at normal incidence. Most of our measurements were therefore performed on fibres whose meridian was approximately horizontal and which produced a reasonably symmetrical diffraction pattern at normal incidence.

The effect of refraction on an ω-scan was discussed above, and the use of a focussed beam not only reduces the refraction effect but also has two important practical advantages:

1) All of the incident light hits the fibre and the total intensity of each diffraction spot can be recorded directly using a photodiode without the need for an imaging lens. Hence *absolute* values of diffraction efficiencies can readily be determined.

2) Only a very short segment (~ 50 μm) of the muscle fibre is illuminated by a focussed beam. As was shown by Brenner (1985), it is much more feasible to find well-ordered striations in such a short segment than in one 1 mm or so long, which would be necessary for an unfocussed beam.

In the experiment, the photodiodes were placed about 12.5 cm away from the focal point so as to intercept the meridional spots of diameter about 3 mm. Each diode was positioned so that when the Bragg condition for its order was satisfied the spot fell on the centre of the diode. As the cell was rotated the angle of diffraction θ_l for order l varied according to the grating formula,

$$d(\sin\omega + \sin(\theta_l - \omega)) = l\lambda\,. \tag{32}$$

Fixing the position of each photodiode therefore meant that for some extreme angles of incidence the diffraction spot missed the diode, but by centring the diffraction spot at the Bragg angle we ensured that each diode gave a true reading of the diffracted intensity in the most important region either side of the Bragg peak. Any artefacts due to diode positioning were therefore confined to incident angles well away from the Bragg angle, where the weak diffracted intenstiy is in any case of little interest.

We believe that the use of a focussed laser beam was very important in obtaining reliable quantitative diffraction data. Note, however, that this procedure does possess two possible disadvantages:

1) When the optical cell is rotated away from normal incidence, refraction by the fluid in the parallel-sided cell displaces the beam so that it no longer passes through the centre of rotation. This causes the laser spot to scan along the fibre and may therefore produce artefacts in an ω-scan if the fibre order varies along its length. To counteract this effect, we offset the fibre from the centre of rotation by about 1 mm along the beam direction at normal incidence. When the cell was rotated the displacement due to the offset almost exactly cancelled that due to refraction, and the excursion of the laser spot along the fibre during an ω-scan was thus limited to less than ± 100 μm.

2) As discussed in the previous section, the use of a focussed laser beam introduces a range of incident angles by virtue of the cone of focussed rays. Hence an ω-scan obtained with a focussed beam incorporates some degree of angular averaging because the angle of incidence ω is no longer sharply defined. In our experiments we used a lens of focal length 40 mm to produce a focal spot of about 50 μm diameter on the muscle fibre. A defocussed spot of about 3 cm diameter was found on a screen placed 99 cm behind the sample cell, and this implies that the beam divergence was about 1.7°. This is probably an overestimate of the effective beam divergence because of the Gaussian profile of the laser beam.

Results and discussion

We have obtained results from several muscle fibres which illustrate quite well the coupled-wave effects described in the theoretical section. Some of our best results are shown in Fig. 12a for a fibre of thickness 71 μm and sarcomere length 3.04 μm. Curve (*i*) is an ω-scan for the zeroth-order beam, which passes straight through the fibre. The intensity of this order is significantly reduced by diffraction in the region of the first-order Bragg angle on either side of normal incidence. Curves (*ii*) and (*iii*) show the signals from the photodiodes monitoring the two first-order diffraction spots ($l = \pm 1$ in the theory); the light lost from the incident beam does indeed appear in the diffraction orders, and the peak first-order diffraction efficiency in this case is 34%. At higher angles of incidence some of the incident beam is diffracted into the third order, shown in curve (*iv*), whilst the second-order diffracted intensity is virtually zero for all angles of incidence at the sarcomere length of 3.04 μm used here.

Figure 12b presents the theoretical ω-scans corresponding to Fig. 12a calculated using the seven-beam coupled-wave approximation for a medium with straight striations. Curve (*i*) illustrates the behaviour of the zeroth-order beam, whilst (*ii*) and (*iii*) show the diffraction efficiencies for the first-order diffraction spots. The peak first-order diffraction efficiency is predicted to be 36%, which is in remarkably good agreement with the experimental value. Furthermore, the theoretical second-order diffraction efficiency almost vanishes at the sarcomere length of 3.04 μm, and this is also borne out by experiment. On the other hand, the comparison of theory with experiment for the third order, curve (*iv*), is much less satisfactory: whereas the theoretical peak in Fig. 12b is very narrow with a maximum diffraction efficiency of 53% at the third-order Bragg angle, the experimental ω-scan in Fig. 12a shows a much broader and rather weaker peak with a maximum of only 15%.

Much better agreement between theory and experiment is obtained once we introduce a small amount of curvature into the striation pattern. Close examination of the experimental first-order peaks in Fig. 12a reveals two of the characteristic effects of curvature which were illustrated in the theoretical ω-scans of Fig. 6. First of all, the minima either side of the Bragg peak are filled in, which may be due to a bow in the striation pattern as illustrated in Fig. 6b. Secondly, there is a distinct asymmetry in the heights of the subsidiary maxima similar to that caused by the full-wave ripple in Fig. 6e. We have therefore repeated the theoretical seven-beam calculation incorporating both a bow (of amplitude 0.75 μm) and a ripple (of amplitude 0.15 μm) into the striation pattern. The resulting ω-scans in the presence of these curved striations are shown in Fig. 12c. The similarity of the first-order peaks to the experimental data in Fig. 12a is most striking: both the asymmetry and the depth of modulation of the subsidiary maxima are now well reproduced. As one might expect, the introduction of a small amount of curvature into the striations has a much greater effect on the third-order peak, which is considerably broadened and reduced in intensity. The shape of this peak is very sensitive to the precise function used to represent the curvature of the striations, so Fig. 12c should only be regarded as being *suggestive* of the type of curvature which may have been present in the actual muscle fibre which produced Fig. 12a. The overall agreement between theory and experiment is nonetheless very good, and lends strong sup-

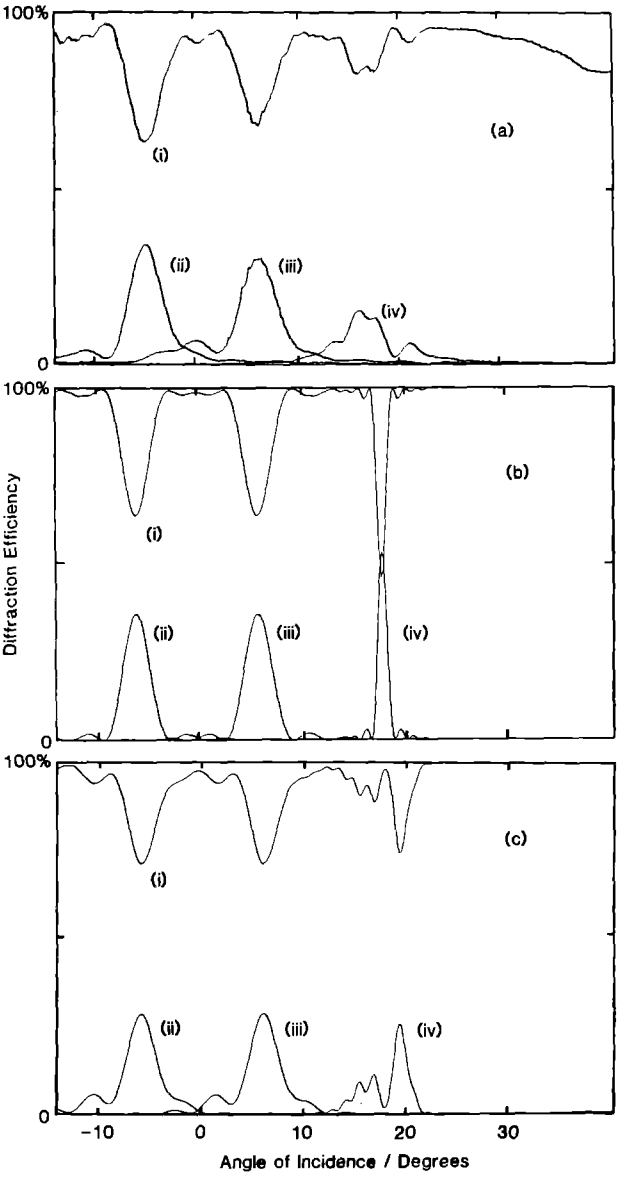

Fig. 12a–c. Experimental ω-scans for a fibre of thickness 71 μm with sarcomere length 3.04 μm are shown in **a**. Curve (*i*) shows the transmission efficiency for the zeroth-order beam. Curves (*ii*) and (*iii*) show the first-order diffraction efficiencies ($l = \pm 1$ in the theory), which reach 34% at the Bragg angle. Curve (*iv*) shows the diffraction efficiency for the third order. Note that the second-order diffraction efficiency is virtually zero at the sarcomere length used here. **b** shows the theoretical ω-scans corresponding to **a** calculated using the seven-beam approximation for a medium with *perfectly straight* striations. The peak diffraction efficiencies are 36% for the first order and 53% for the third order. **c** shows the corresponding theoretical ω-scans for a medium with *curved* striations: a bow of amplitude 0.75 μm together with a full-wave ripple of amplitude 0.15 μm. Compared to **b** the shape of the first-order peaks (*ii*) and (*iii*) is much better reproduced, and the irregular broadening of the third-order peak (*iv*) is similar to the experimental data in **a**

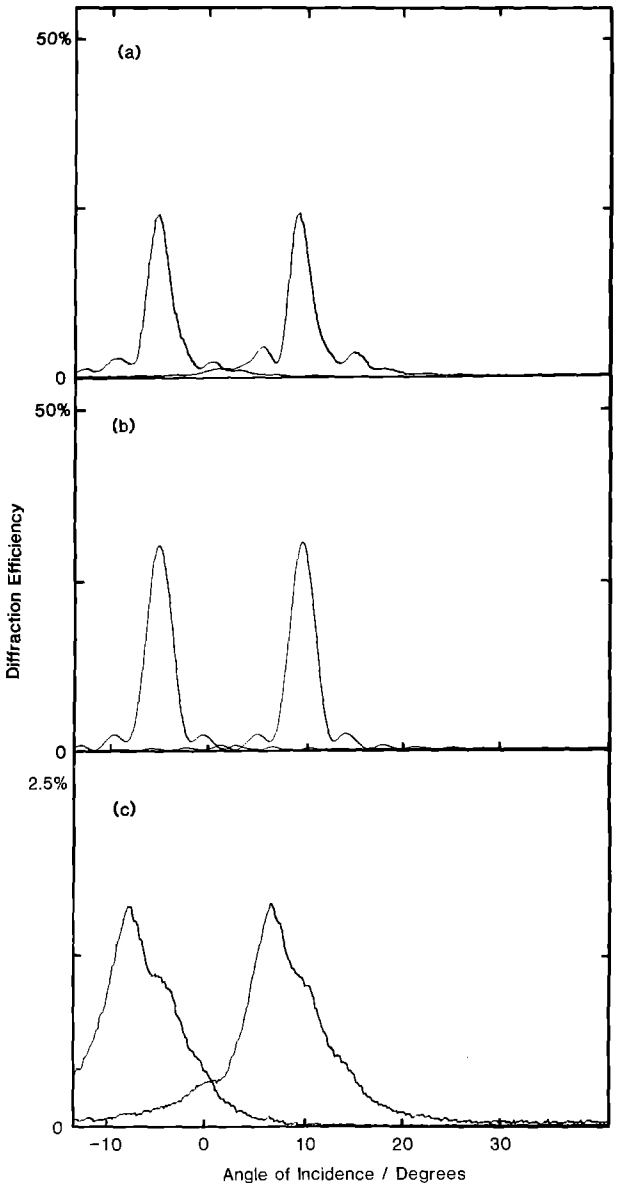

Fig. 13a–c. Experimental first order ω-scans for a fibre of thickness 58 μm with sarcomere length 2.45 μm are shown in **a**. The maximum diffraction efficiency is 24%. **b** shows the corresponding theoretical ω-scans calculated using the seven-beam approximation for striations containing a bow of amplitude 0.35 μm and with 1.6 μm of skew. Experimental first-order ω-scans for the same fibre but using an unfocussed laser beam, are shown in **c**

port to the coupled-wave theory for optical diffraction from single muscle fibres.

Figure 13a shows the experimental ω-scans for the two first-order diffraction spots for a fibre of thickness 58 μm with sarcomere length 2.45 μm. The peaks here are more symmetrical than those in Fig. 12a, but there is still a significant filling in of the minima, perhaps due to some bowing of the striations coupled with a certain amount of angular averaging from the focussed beam. There is also some evidence of skew for this fibre, as both peaks are displaced from the theoretical Bragg angle (Rüdel and Zite-Ferenczy 1979; Gilliar et al. 1984). Theoretical peaks for slightly bowed striations (amplitude 0.35 μm) with 1.6 μm of skew were calculated using the seven-beam theory and are shown in Fig. 13b. The maximum theoretical diffraction efficiency is 30% compared to the observed value of 24%. Experimental results for the same fibre using an *unfocussed* laser beam are shown in Fig. 13c. The peaks are now much broader, and the subsidiary maxima are reduced to barely perceptible bumps. The broadening of the Bragg peak itself is far more severe than could be accounted for by refraction due to the cylindrical fibre (cf. Fig. 8). This may be because the curvature of the striations varies along the millimetre length of fibre illuminated by the unfocussed laser beam (Brenner 1985). The resultant ω-scan is then the superposition of the ω-scans for segments with different curvature, which causes the sharp angular dependence for the single 50 μm segment in Fig. 13a to be lost. Note that the vertical scale for Fig. 13c does not reflect the true diffraction efficiency of the fibre, as only part of the incident beam hit the fibre and only part of the diffraction line was intercepted by the photodiode. Comparison of Fig. 13a with Fig. 13c therefore clearly demonstrates the practical advantages of using a focussed beam for our diffraction measurements.

In our experience only a small percentage of muscle fibres produce ω-scans as nearly ideal as Fig. 12a or Fig. 13a. The sensitivity of the ω-scans to even the slightest curvature of the striations is a major practical difficulty in the study of optical diffraction by muscle fibres. Furthermore, changes in the curvature of the striations may contribute to intensity changes in other optical experiments. One example is the investigation of transparency changes for whole muscle by Hill (1953a, b) and Flitney (1975) together with the more recent work on single fibres by Leung and Cheung (1988). These workers observed changes in muscle transparency and diffracted intensity on stretching or activating muscle. Our work suggests that such intensity changes might be produced by changes in the striation pattern: to verify this, one would need record ω-scans before and after the physiological state of the muscle is altered.

Our work may also be relevant to studies of changes in the *birefringence* of muscle (Haskell et al. 1989, Chen et al. 1989, Peckham and Irving 1989): since the refractive index is different for the *E*- and *O*-rays their intensities will be affected differently by changes in the curvature of the striations. More theoretical and experimental work is needed to clarify this point.

Conclusions

We have presented a detailed theoretical model for optical diffraction by well-ordered muscle fibres based on Kogelnik's coupled-wave theory. Experimental studies of diffraction of a focussed laser beam have yielded first-order diffraction efficiencies as high as 34%, in good agreement with the theoretical prediction. This demonstrates that coupled-wave effects are indeed important in optical diffraction by well-ordered single muscle fibres. The theoretical model shows that the diffraction efficiency is extremely sensitive to any curvature in the striation pattern, and this is borne out by our experimental results, which exhibit the characteristic features of bows and rip-

ples in the striations. This observation has wider implications for the interpretation of other optical experiments in muscle physiology, such as changes in muscle transparency and birefringence.

Acknowledgements. We are grateful to Messrs. J. Harling and C. Hardman for their expert technical assistance and to Dr. D.W. Thomas for the use of an Abbé refractometer. We also with to thank Profs. P.J. Butler, J. Callow, D.C. Colley and G.C. Morrison for their support.

References

Baskin RJ, Lieber RL, Oba T, Yeh Y (1981) Intensity of light diffraction from striated muscle as a function of incident angle. Biophys J 36:759–773

Berovic N, Thomas N, Thornhill RA, Vaughan JM (1989) Observation of Brillouin scattering from single muscle fibres. Eur Biophys J 17:69–74

Blinks JR (1965) Influence of osmotic strength on cross-section and volume of isolated single muscle fibres. J Physiol 177:42–57

Bowman W (1840) On the minute structure and movements of voluntary muscle. Phil Trans R Soc 457–501

Brenner B (1983) Technique for stabilizing the striation pattern in maximally calcium-activated skinned rabbit psoas fibres. Biophys J 41:99–102

Brenner B (1985) Sarcomeric domain organization within single skinned rabbit psoas fibres and its effect on laser light diffraction patterns. Biophys J 48:967–982

Brenner B, Yu LC (1985) Equatorial X-ray diffraction in single skinned rabbit psoas fibres. Biophys J 48:829–834

Buchthal F, Knappeis GG (1940) Diffraction spectra and minute structure of the cross-striated muscle fibre. Skand Arch 83: 283–307

Chen JS, Baskin RJ, Burton K, Shen S, Yeh Y (1989) Polarization states of light. Biophys J 56:595–605

Cleworth D, Edman KAP (1969) Laser diffraction studies on single skeletal muscle fibers. Science 163:296–298

Cowley JM (1975) Diffraction physics. North-Holland, Amsterdam

Flitney FW (1975) Light scattering associated with tension changes in the short-range elastic component of resting frog muscle. J Physiol 244:1–14

Fujime S, Yoshino S (1978) Optical diffraction study of muscle fibers I. Biophys Chem 8:305–315

Gilliar WG, Bickel WS, Bailey WF (1984) Light diffraction studies of single muscle fibres as a function of fibre rotation. Biophys J 45:1159–1165

Hariharan P (1984) Optical holography. Cambridge University Press, Cambridge

Haskell RC, Carlson FD, Blank PS (1989) Form birefringence of muscle. Biophys J 56:401–413

Hill DK (1953a) The optical properties of resting striated muscle. J Physiol 119:489–500

Hill DK (1953b) The effect of stimulation on the diffraction of light by striated muscle. J Physiol 119:501–512

Huxley AF (1990) A theoretical treatment of diffraction of light by a striated muscle fibre. Proc R Soc Lond B 241:65–71

Huxley AF, Niedergerke R (1958) Measurement of the striations of isolated muscle fibres with the interference microscope. J Physiol 144:403–425

Huxley HE, Hanson J (1957) Quantitative studies on the structure of cross-striated myofibrils. Biochim Biophys Acta 23:229–249

Kawai M, Kuntz ID (1973) Optical diffraction studies of muscle fibers. Biophys J 13:857–875

Kogelnik H (1967) Coupled wave theory for thick hologram gratings. Bell System Tech J 48:2909–2947

Leung AF, Cheung MK (1988) Decrease in light diffraction intensity of contracting muscle fibres. Eur Biophys J 15:359–368

Magnusson R, Gaylord TK (1977) Analysis of multiwave diffraction of thick gratings. J Opt Soc Am 67:1165–1170

Marikhin VA, Myasnikova LP (1970) Diffraction patterns of muscle fibres (in Russian). Tsitologiya 12:1231–1236

Peckham M, Irving M (1989) Myosin cross-bridge orientation in demembranated muscle fibres studied by birefringence and X-ray diffraction measurements. J Mol Biol 210:113–126

Ranvier L (1874) Du spectre produit par les muscles striés. Arch Physiol 6:774–780

Rüdel R, Zite-Ferenczy F (1979) Interpretation of light diffraction by cross-striated muscle as Bragg reflexion of light by the lattice of contractile proteins. J Physiol 290:317–330

Rüdel R, Zite-Ferenczy F (1980) Efficiency of light diffraction by cross-striated muscle fibers under stretch and during isometric contraction. Biophys J 30:507–516

Sandow A (1936) Diffraction patterns of the frog sartorius and sarcomere behaviour under stretch. J Cell Comp Physiol:37–54

Wang K, Wright J (1988) Architecture of the sarcomere matrix of skeletal muscle. J Cell Biol 107:2199–2212